Electric Power Systems Research 212 (2022) 108584

Contents lists available at ScienceDirect

Electric Power Systems Research

journal homepage: www.elsevier.com/locate/epsr

Optimal pump scheduling in multi-phase distribution networks using Benders decomposition☆

Krishna Sandeep Ayyagari, Nikolaos Gatsis *

Department of Electrical and Computer Engineering, The University of Texas at San Antonio, United States of America

ARTICLE INFO

Keywords:
Distribution networks
Optimal power flow
Optimal water flow
Mixed-integer program
Semidefinite relaxation
Successive approximation
Benders decomposition

ABSTRACT

With the growing adoption of renewable energy resources in the power grid, co-optimizing the operation of water and power distribution networks (WDNs and PDNs) increases the flexibility of both systems. The optimal water power flow problem (OWPF) is formulated to manage resource utilization across the WDNs and multi-phase PDNs. The nonlinear WDN hydraulic constraints and PDN ac power flow equations render the OWPF problem nonconvex. This paper formulates a convex optimal water power flow (C-OWPF) problem adopting successive approximations in WDNs and branch-flow relaxations in PDNs. The C-OWPF problem is a mixed-integer semidefinite program, which is computationally challenging even for small instances. Additionally, privacy considerations of WDN and PDN operators motivate the need for solving the C-OWPF in a distributed fashion. This paper develops a C-OWPF solver based on Benders decomposition that overcomes computational complexity challenges and preserve the privacy of the respective operators. The merits of the Benders decomposition-based solver are demonstrated on the IEEE 4-bus PDN coupled with a 3-node WDN and the IEEE 123-bus PDN coupled with the 36-node WDN.

1. Introduction

Power distribution networks (PDNs) and water distribution networks (WDNs) are interdependent critical infrastructures, although traditionally operated independently. The physical coupling is due to the significant electrical load presented by water pumps, which provide the necessary pressure for the water to be delivered at the points of consumption [1]. The optimal water-power flow (OWPF) problem aims at jointly managing resources at both networks, ranging from distributed energy resources at PDNs to pumps and tanks at WDNs. Benefits include energy conservation and reliability of power and water delivery. The OWPF is a challenging optimization problem due to the nonconvexities of the power flow equations, and the hydraulics governing water flows in pipes and pumps. A collaborative effort between PDN and WDN operators provides an excellent opportunity to reduce peak energy demand, thereby minimizing both active power losses and violations of PDN security constraints such as voltage limits [2,3].

The joint management of WDNs and PDNs has been investigated in e.g., [3–7] and references therein. The majority of existing works such as [5–7] deal with single-phase PDN models. Furthermore, solving the OWPF problem in a centralized fashion poses data organization and privacy concerns in addition to increasing computational burden. To address the aforementioned issues, [6,7] develop distributed algorithms for joint management of WDNs and single-phase PDNs. Most importantly, it is necessary to model pump scheduling in multi-phase power distribution networks because the pumps in WDNs are connected to multi-phase induction motors that operate in an unbalanced manner [8] due to unbalanced voltage conditions on the motor side [9] or mechanical defects within the pump.

Favorable computation times have been reported for the branch-flow model with semidefinite programming (BFM-SDP) to solve multi-phase optimal power flow problems (OPF) with a few thousand nodes [10,11]. However, solving multi-period SDPs with discrete decision variables remains a significant computational challenge, as has been reported in the literature; see e.g., [12]. The present work is concerned with such hard optimization problems arising from WDN pump *on/off* scheduling in multi-phase PDNs.

To the best of our knowledge, no existing approaches consider WDNs integrated with multi-phase PDNs, with the exception of the work in [4]. In the latter, the pump *on/off* schedules and water flow directions are assumed known a priori, which eliminates the combinatorial aspects of the problem. In addition, the pump head loss is modeled as linear, which lends itself to computational efficiency advantages, though the physics dictate polynomial or power laws.

☆ This work is supported by the U.S. NSF Grant CAREER-1847125.

* Corresponding author.
E-mail addresses: krishnasandeep.ayyagari@utsa.edu (K.S. Ayyagari), nikolaos.gatsis@utsa.edu (N. Gatsis).

https://doi.org/10.1016/j.epsr.2022.108584
Received 3 October 2021; Received in revised form 18 April 2022; Accepted 2 July 2022
Available online 18 July 2022

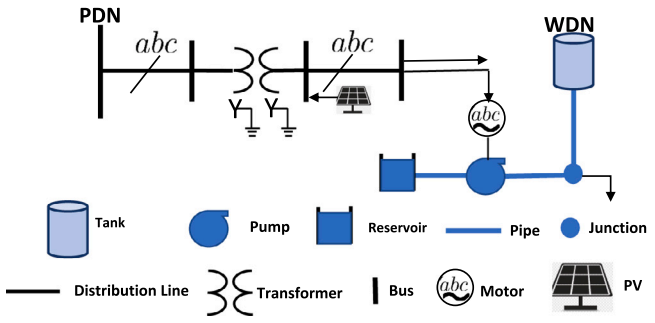

Fig. 1. Power (left) and water (right) distribution networks.

Our previous work on WDN operations [13,14] has contributed linearizations through novel monomial approximations of the WDN hydraulics, and the coupling with the PDNs incorporating pump operations in WDNs using integer variables is explored in [2]. Moreover, [2] omitted multi-phase PDNs, and the OWPF problem is solved as a mixed-integer quadratically constrained quadratic program (MIQCQP) in a centralized fashion.

The contributions of this paper are as follows: (1) We expand our previous work in [2] to multi-phase PDNs formulating and approaching the OWPF in an effort to lift certain limitations in the existing literature. Specifically, the *on/off* scheduling of pumps is modeled using appropriate binary variables and is coupled with the BFM-SDP relaxation for the three-phase OPF. By applying the recent monomial approximations to the nonlinear hydraulics and dropping the SDP rank-1 constraints for the OPF, the overall formulation amounts to a mixed-integer semidefinite programming problem called C-OWPF. (2) To ensure privacy and simultaneously respect the interdependencies between WDNs and PDNs, an efficient solver based on Benders decomposition is developed. The problem separation provides an attractive approach to integrate the binary decision variables of WDNs in the OPF and sidesteps the intractability issues with mixed-integer semidefinite programming. Specifically, the resulting *master* problem is solved by the WDN operator yielding mixed-integer linear programming formulations. The *subproblem* is an SDP problem that pertains to the PDN operator, but does not include binary variables. (3) The Benders-based C-OWPF solver is assessed in terms of joint objective improvements compared to a traditional rule-based decoupled approach implemented in the benchmark WDN analysis software EPANET [15]. (4) The Benders-based C-OWPF solver is also compared to a centralized C-OWPF solver which adopts the *LinDist3Flow* approximation of the power flow equations. The performance of the Benders-based C-OWPF solver in terms of accuracy and feasibility of the nonlinear hydraulics and power flows is analyzed as well. The IEEE 123-bus PDN is coupled with a 36-node WDN to this end.

The organization of the paper is given next. Section 2 discusses the modeling of WDNs and PDNs and the formulation of MISDP-based C-OWPF problem. Section 3 presents the proposed Benders-based solver. The simulation results are presented in Section 4, and the conclusions are drawn in Section 5.

2. WDN and PDN models

This section details the mathematical models for water and power distribution networks as shown in Fig. 1. In this section, we first describe the nonconvex optimal water flow problem (OWF) and apply successive approximations techniques leveraging our works [2], [13], and [14] to convexify the problem. We then adopt the BFM-SDP relaxation [10] for unbalanced distribution networks considering inverter-interfaced photovoltaic resources (PVs) and formulate the multi-period OWPF problem.

Water Distribution Network Model: The WDN is modeled by a directed graph $(\mathcal{M},\mathcal{L})$ where $\mathcal{M}=\{0,\ldots,M\}$ is a set of $M+1$ nodes with $\mathcal{M}=\mathcal{J}\bigcup\mathcal{R}\bigcup\mathcal{K}$, and $\mathcal{J}$, $\mathcal{R}$, and $\mathcal{K}$ respectively denote sets of junctions, reservoirs, and tanks. Let $\mathcal{L}\subseteq\mathcal{M}\times\mathcal{M}$ be the set of links connecting the nodes partitioned as $\mathcal{L}=\mathcal{P}\bigcup\mathcal{W}$, where $\mathcal{P}$ and $\mathcal{W}$ respectively denote the sets of pumps and pipes. Also, in this work, we assume that the pumps are connected to fixed-speed motors, i.e., they are fixed-speed pumps (FSPs) with constant wire-to-water efficiency η_{ij}^{ww}.

The WDN operation is optimized over a horizon $\mathcal{T}=\{1,\ldots,T\}$, with δ representing the time interval between two consecutive time periods. It is worth noting that the optimization problem yields the directions of water flow in pipes. Next, we present the mathematical model of WDN operational constraints for $t\in\mathcal{T}$:

$$\sum_{i:ij\in\mathcal{L}} f_{ij,t}-\sum_{k:jk\in\mathcal{L}} f_{jk,t}=d_{j,t},\quad j\in\mathcal{J} \tag{1a}$$

$$h_{i,t}-h_{j,t}=A_{ij}|f_{ij,t}|^{\mu-1}f_{ij,t},\quad ij\in\mathcal{W} \tag{1b}$$

$$h_{k,t}=h_{k,t-1}+\frac{\delta_t}{A_k}\left(\sum_{i:ik\in\mathcal{L}} f_{ik,t}-\sum_{j:jk\in\mathcal{L}} f_{jk,t}\right),k\in\mathcal{K} \tag{1c}$$

$$h_{i,t}-h_{j,t}=\left\{\begin{array}{l}-(h_{0,ij}-\sigma_{ij}f_{ij,t}^{\nu_{ij}}),\ \text{if } x_{ij,t}=1\\ \text{unconstrained},\ \text{if } x_{ij,t}=0, ij\in\mathcal{P}\end{array}\right\} \tag{1d}$$

$$f_{ij,\min}\,x_{ij,t}\le f_{ij,t}\le f_{ij,\max}\,x_{ij,t},\quad ij\in\mathcal{P} \tag{1e}$$

$$p_{ij,t}^{\mathrm{pump}}=\frac{\rho g}{\eta_{ij,t}^{\mathrm{ww}}}|h_{i,t}-h_{j,t}|f_{ij,t},\quad ij\in\mathcal{P} \tag{1f}$$

$$h_{i,t}=h_i^{\mathrm{R}},\quad i\in\mathcal{R} \tag{1g}$$

$$h_{j,\min}\le h_{j,t}\le h_{j,\max},\quad j\in\mathcal{J},\mathcal{K} \tag{1h}$$

Constraint (1a) enforces the mass conservation at junction $j\in\mathcal{J}$ at time t, where $d_{j,t}$ is the estimated water demand at time t. Constraint (1b) formulates the head loss in pipe $ij\in\mathcal{P}^p$ which is approximated by the empirical Hazen–Williams equation [15], where $A_{ij}=4.727C_{ij}^{-1.852}\hat{d}_{ij}^{-4.871}\hat{l}_{ij}$; $\hat{d}_{ij}$ and $\hat{l}_{ij}$ are respectively the diameter and length of a circular pipe; C_{ij} is the Hazen–Williams roughness coefficient (unitless); μ is the flow exponent; and $f_{ij,t}$ is the volumetric flow rate through pipe $ij\in\mathcal{W}$. Constraint (1c) models the water tank head dynamics for tank $k\in\mathcal{K}$ with cross-sectional area A_k and initial head $h_{k,0}$ (assumed to be known).

Constraint (1d) models the head loss across the FSP connected between nodes i and j and is modeled according to ([15], Ch. 3), where $h_{0,ij}$ is the shutoff head for the pump, σ_{ij},ν_{ij} are the pump curve coefficients evaluated at nominal speed, $f_{ij,t}$ is the water flow through the pump and $x_{ij,t}$ is the binary variable to indicate whether the pump $ij\in\mathcal{P}$ is running at time t. Also note that the head loss of FSP $h_{ij,t}$ in (1d) is negative when the pump is on, which means that head gain is provided across the pump. The pump flow is constrained by (1e). The binary variable $x_{ij,t}$ is set to 1 when pump $(ij)\in\mathcal{P}$ is on at time t and the constraint (1d) is active; otherwise no constraint exists between $h_{i,t}$ and $h_{j,t}$.

A more convenient mathematical formulation is needed to capture the FSP on/off status and operation logic given by (1d) and (1e). This task is accomplished using the big-M technique to rewrite the aforementioned constraints.

$$\begin{aligned}M(x_{ij,t}-1)\le h_{ij,t}+[h_{0,ij}-\sigma_{ij}(f_{ij,t})^{\nu_{ij}}]\\ \le M(1-x_{ij,t})\end{aligned} \tag{2a}$$

$$h_{i,t}-h_{j,t}=h_{ij,t} \tag{2b}$$

$$h_{ij,t}\le 0 \tag{2c}$$

$$x_{ij,t}\in\{0,1\},\quad ij\in\mathcal{P} \tag{2d}$$

Eq. (2) corresponds to FSP operation, where $h_{ij,t}$ is the auxiliary variable that represents pump head loss (1d).

The FSP power consumption is captured in (1f), where ρ and g respectively denote the water density and standard gravity coefficient. The fixed reservoir head is given by (1g) which is operational constraint and the head of the remaining nodes is constrained by (1h). Also, for simplicity let $\gamma_{ij} = \frac{\rho g}{\eta_{ij}^{\text{ww}}}, \quad ij \in \mathcal{P}$.

The optimal water flow problem is described next. In this work, the objective is to minimize the pump power consumption in WDNs:

$$\Gamma_{ij,t}^{\text{pump}}(f_{ij,t}) = p_{ij,t}^{\text{pump}}, \quad ij \in \mathcal{P} \tag{3}$$

and the objective $\Gamma_{ij,t}^{\text{pump}}(.)$ is written as

$$\Gamma_{ij,t}^{\text{pump}}(.) = \gamma_{ij}|h_{ij,t}|f_{ij,t} \tag{4}$$

where $h_{ij,t}$ is given by (2b).

Other pertinent objectives can also be considered, such as water consumption costs, pump maintenance costs, and water delivery costs incurred by the water utility operator [16,17]. However, the pump power is typically the main contributing factor in WDN costs. Therefore, this work focuses on minimizing pump power.

The optimal water flow problem (OWF) is formulated as

$$\text{(P1)} \ \min \quad \sum_{t=1}^{T}\left[\lambda_t^{\text{WDN}} \sum_{ij\in\mathcal{P}} \Gamma_{ij,t}^{\text{pump}}\right] \tag{5a}$$

$$\text{over} \quad \{p_{ij,t}^{\text{pump}}, f_{ij,t}\}_{t=1}^{T}, \quad \{h_{ij,t}, h_{j,t}, x_{ij,t}\}_{t=1}^{T}, \quad ij \in \mathcal{L}, j \in \mathcal{M}$$

$$\text{subj. to} \quad \text{(1a)–(1c), (1f)–(1h), (2)} \tag{5b}$$

where λ_t^{WDN} denotes the time-varying price of electricity for the WDN.

The OWF (P1) is a mixed-integer nonlinear program (MINLP). The nonconvexities stem from the head loss models of pipes and pumps (1b) and (1d). Also, the objective corresponding to pump power consumption (1f) is nonconvex. To bypass the nonconvexity issues, we utilize the monomial approximations in [13,14]. Specifically, the nonlinear head loss model for pipes and pumps (1b) and (1d) are respectively approximated by linear forms around given points (flow values) as follows:

$$\hat{h}_{ij,t} = \kappa_{ij,t} + f_{ij,t}, \ ij \in \mathcal{W}, \ t \in \mathcal{T} \tag{6a}$$

$$\hat{h}_{ij,t} = (\tau_{ij,t} + \varphi_{ij,t} f_{ij,t}), \ ij \in \mathcal{P}, \ t \in \mathcal{T} \tag{6b}$$

Eq. (6) is used to iteratively approximate (1b) and (1d), by updating $\kappa_{ij,t}$ and $\varphi_{ij,t}$. In particular, (6) replaces (1b) and (1d), the resulting optimization problem is solved, and the produced values $f_{ij,t}$ are used to update $\kappa_{ij,t}$ and $\varphi_{ij,t}$ via $\kappa_{ij,t} = f_{ij,t}(A_{ij}|f_{ij,t}|^{\mu-1} - 1)$ and $\varphi_{ij,t} = \sigma_{ij} {f_{ij,t}}^{\nu_{ij}-1}$ with $\tau_{ij,t} = -h_{0,ij}$.

Also, constraint (6b) is valid when the pump is in the on state. Therefore we replace the nonlinear pump head loss constraint in (2a) with its corresponding linear form (6b) while implementing big-M for the pump head loss, which is not shown here due to space limitations.

Attention is then turned to the nonlinear FSP power consumption. Substituting (1d) (when $x_{ij,t} = 1$) in (1f), the FSP power is given as

$$p_{ij,t}^{\text{pump}}(f_{ij,t}) = \gamma_{ij}\left(h_{0,ij} f_{ij,t} - \sigma_{ij} {f_{ij,t}}^{\nu_{ij}+1}\right), \ ij \in \mathcal{P} \tag{7}$$

Since $(p^{\text{pump}}(f_{ij,t}))'' \leq 0$, the FSP power consumption from (7) is concave. Hence, we devise the linear upper bound to (7) as follows

$$\hat{p}_{ij,t}^{\text{pump}}(f_{ij,t}) = \gamma_{ij}\left(\alpha_{ij,t} f_{ij,t} + \beta_{ij,t} x_{ij,t}\right) \tag{8}$$

where $\alpha_{ij,t}$, $\beta_{ij,t}$ are constants which are computed from the previous iteration pump flows $f_{ij,t}$. This entails $\hat{p}_{ij,t}^{\text{pump}}$, $ij \in \mathcal{P}$ to be linear as in (8).

The C-OWF problem (convex OWF) (P2) is stated as follows

$$\text{(P2)} \quad \min \quad \sum_{t=1}^{T}\left[\lambda_t^{\text{WDN}} \sum_{ij\in\mathcal{P}} \tilde{\Gamma}_{ij,t}^{\text{pump}}\right] \tag{9a}$$

$$\text{over} \quad \{f_{ij,t}, \hat{p}_{ij,t}^{\text{pump}}, \hat{h}_{ij,t}, h_{j,t}, x_{ij,t}\}_{t=1}^{T}, \quad ij \in \mathcal{L}, \mathcal{P}, j \in \mathcal{M} \tag{9b}$$

$$\text{subj. to} \quad \text{(1a), (1c), (1g), (1h), (2), (6), (8)} \tag{9c}$$

with $\tilde{\Gamma}_{ij,t}^{\text{pump}} = \hat{p}_{ij,t}^{\text{pump}}$. The C-OWF (P2) is a mixed-integer linear program (MILP) and can be solved in a iterative fashion as given in [2]. Specifically, the parameters $\kappa_{ij,t}$, $\tau_{ij,t}$, $\psi_{ij,t}$, $\alpha_{ij,t}$, and $\beta_{ij,t}$ ($ij \in \mathcal{L}$) in (P2), are all constants which are evaluated from the flow values of the previous iteration. We use the term convex in C-OWF to emphasize that *the continuous part of (9) is linear and hence convex*.

Power Distribution Network Model: A multi-phase radial PDN is modeled using a directed graph $(\mathcal{N}, \mathcal{E})$, where $\mathcal{N}$ is the set of buses and $\mathcal{E} \subseteq \mathcal{N}\times\mathcal{N}$ is set of distribution lines or transformers. Furthermore, partition $\mathcal{N}$ as $\mathcal{N} = \mathcal{N}_+ \cup \{0\}$, where $\mathcal{N}_+$ and $\{0\}$ are respectively the sets of user buses and the slack (root) bus. Furthermore, let $\mathcal{N}_+^{\text{pv}} \subseteq \mathcal{N}_+$ represent the set of PV buses while $\mathcal{N}_+^{\text{pump}} \subseteq \mathcal{N}_+$ and $\mathcal{N}_+^{c} \subseteq \mathcal{N}_+$ respectively represent set of buses connected to pumps and loads. For a bus $n \in \mathcal{N}$, an ordered pair (n, m) (interchangeably, $n \to m$) belongs to set $\mathcal{E}$. For the sake of exposition, we assume that the full set of three phases $\{a, b, c\}$ are present in all buses and distribution lines. The extension to networks with missing phases can be carried out using more elaborate notation.

Let $v_{n,t}$, $i_{nm,t} \in \mathbb{C}^3$ and $Z_{nm} \in \mathbb{C}^{3\times3}$ respectively denote the vector of phase voltages at bus $n \in \mathcal{N}$ at time t, the vector of line currents, and the series impedance of the edge $(n, m) \in \mathcal{E}$ (neglecting the shunt admittance). The BFM-SDP constraints are derived using Ohms' law [10]. The voltage drop on $(n, m) \in \mathcal{E}$ is

$$v_{m,t} = v_{n,t} - Z_{nm} i_{nm,t}, (n, m) \in \mathcal{E} \quad t \in \mathcal{T} \tag{10}$$

where Z_{nm} is the series impedance of a transmission line [9] or the inverse of the per-unit shunt admittance for a grounded-wye grounded-wye transformer [11,18].

Introduce the auxiliary variables $V_{n,t} = v_{n,t}\bar{v}_{n,t}$, $V_{m,t} = v_{m,t}\bar{v}_{m,t}, (n, m) \in \mathcal{N}\times\mathcal{N}$; $S_{nm,t} = v_{n,t}\bar{i}_{nm,t}, (n, m) \in \mathcal{E}$; and $I_{nm,t} = i_{nm,t}\bar{i}_{nm,t}, (n, m) \in \mathcal{E}$. Upon multiplying both sides of (10) by conjugate transposes $(\bar{.})$, i.e., $\bar{v}_{n,t}$ on the left and $(\bar{v}_{n,t} - \bar{i}_{nm,t}\bar{Z}_{nm})$ on the right, (10) can be written as

$$V_{m,t} = V_{n,t} - (S_{nm,t}\bar{Z}_{nm} + Z_{nm}\bar{S}_{nm,t}) + Z_{nm} I_{nm,t} \bar{Z}_{nm} \quad (n, m) \in \mathcal{E}, \quad t \in \mathcal{T} \tag{11}$$

To formulate the power balance at bus m, for each $n \to m \to k$, (10) is multiplied by $\bar{i}_{nm}$:

$$v_{m,t}\bar{i}_{nm,t} = v_{n,t}\bar{i}_{nm,t} - Z_{nm} i_{nm,t}\bar{i}_{nm,t} \tag{12}$$

$$\Rightarrow v_{m,t}\left[\sum_{(m,k)\in\mathcal{E}} \bar{i}_{mk,t} - \bar{i}_{m,t}\right] = S_{nm,t} - Z_{nm} I_{nm,t}, \quad (n, m) \in \mathcal{E}, \ t \in \mathcal{T} \tag{13}$$

Specifically, $i_{m,t}$ in (13) is the net current injection at bus $m \in \mathcal{N}_+$, which is generically a sum of currents from constant-power sources with net complex power $\mathfrak{s}_{m,t} \in \mathbb{C}^3$ and from constant-admittance elements, such as shunt capacitor banks, with admittance Y_m connected to bus m. The net current is thus $i_{m,t} = \text{diag}(v_{m,t}^*)^{-1}(\mathfrak{s}_{m,t})^* - Y_m v_{m,t}$. Taking conjugate transpose of $i_{m,t}$, substituting in (13), and taking *diagonal* (diag) of matrices to return vectors yields

$$\sum_{(m,k)\in\mathcal{E}} \text{diag}(S_{mk,t}) - s_{m,t} = \text{diag}(S_{nm,t} - Z_{nm} I_{nm,t}) \quad (n, m) \in \mathcal{E}, \ m \in \mathcal{N}_+ \ t \in \mathcal{T} \tag{14}$$

where $s_{m,t} = \mathfrak{s}_{m,t} - \text{diag}(V_{m,t}\bar{Y}_m)$. The matrix variables $V_{n,t}$, $I_{n,t}$, and $S_{nm,t}$ must satisfy $V_{n,t} \odot I_{nm,t} = S_{nm,t} \odot \bar{S}_{nm,t}, (n, m) \in \mathcal{E}, n \in \mathcal{N}_+, t \in \mathcal{T}$, which is ensured by the following positive semidefinite (PSD) and rank-1 constraints:

$$G_{nm,t} = \begin{bmatrix} V_{n,t} & S_{nm,t} \\ \bar{S}_{nm,t} & I_{nm,t} \end{bmatrix} \succeq 0 \tag{15}$$

$$\text{rank}(G_{nm,t}) = 1 \tag{16}$$

Furthermore, the slack bus voltage is set to a nominal value v^{nom} and the remaining bus voltages are constrained by (18):

$$V_{0,t} = v^{\text{nom}}\bar{v}^{\text{nom}},\ t \in \mathcal{T} \tag{17}$$

$$(v_{\min})^2\mathbf{1}_3 \leq \text{diag}(V_{n,t}) \leq (v_{\max})^2\mathbf{1}_3,\ n \in \mathcal{N}_+,\ t \in \mathcal{T} \tag{18}$$

Constraint (18) ensures voltage regulation dictated by ANSI C.84.1.

The nodal injections $\mathfrak{s}_{m,t}$ are analyzed next, according to the presence of a pump, PV inverter, or load. Three-phase induction motors typically drive water pumps in WDNs. This is because three-phase induction motors are easier to design and require less motor maintenance. Specifically, the pumps in WDNs are connected to three-phase induction motors that may operate at unbalanced voltage conditions [19]. Induction motors coupled to pumps may also operate in an unbalanced state due to improper mechanical alignment of the pump and motor or mechanical defects within the pump. Since (8) relates the pump active power consumption and the WDN hydraulics, the complex power consumed by the pump ij connected to bus m at time t, $\hat{s}^{\text{pump}}_{m,ij,t} \in \mathbb{C}^3,\ ij \in \mathcal{P}, m \in \mathcal{N}^{\text{pump}}_+, t \in \mathcal{T}$ is given as

$$\hat{s}^{\text{pump}}_{m,ij,t} = \mathbf{a}_{m,ij} \odot \hat{p}^{\text{pump}}_{m,ij,t} + j\ \mathbf{b}_{m,ij} \odot \mathbf{a}_{m,ij} \odot \hat{p}^{\text{pump}}_{m,ij,t} \tag{19}$$

where $\odot$ is the element-wise multiplication operator. The entries in vector $\mathbf{a}_{m,ij}$ are split the total pump power $\hat{p}^{\text{pump}}_{m,ij,t}$ into three phases with $\mathbf{1}_3^\top\mathbf{a}_{m,ij} = 1$, where $\mathbf{1}_3$ is a 3×1 vector of all ones. The reactive power consumed by the motor coupled to the pump is given by the second term in (19) with $\mathbf{b}_{m,ij} = \tan[\cos^{-1}\text{PF}]\mathbf{1}_3$ where PF is the power factor of the motor. Although this method approximately captures the unbalanced operation of multi-phase induction motors, a more suitable programming model would be to accurately model the induction motor using the methods in [19], Ch. 9.

When distributed PV generation is connected to a bus, it is assumed the PV inverter is oversized to ensure reactive power absorption/consumption during peak solar generation. For a PV at bus $m \in \mathcal{N}^{\text{pv}}_+$, the operational region of a three-phase PV inverters is assumed balanced, that is equal active power is injected per phase, and likewise for reactive power. The active power is uncontrolled and denoted by $\mathsf{p}^{\text{pv}}_{m,t},\ m \in \mathcal{N}_+, t \in \mathcal{T}$. The reactive power per phase is given by

$$|\mathsf{q}^{\text{pv}}_{m,t}| \leq \sqrt{(s^{\text{pv}}_{m,\max})^2 - (\mathsf{p}^{\text{pv}}_{m,t})^2},\ m \in \mathcal{N}^{\text{pv}}_+ \subseteq \mathcal{N}_+ \tag{20}$$

The complex power injected by the PV inverter connected to bus $m \in N^{\text{pv}}_+$ is given by $s^{\text{pv}}_{m,t} = \mathsf{p}^{\text{pv}}_{m,t}\mathbf{1}_3 + j\mathsf{q}^{\text{pv}}_{m,t}\mathbf{1}_3 \in \mathbb{C}^3$. Similarly, the complex power absorbed by the constant-power load connected to bus $m \in N^c_+$ is $s^c_{m,t} = p^c_{m,t} + jq^c_{m,t} \in \mathbb{C}^3$.

Considering the PV model in (20), the constant power demands by pump loads (19) and the uncontrollable loads $s^c_{m,t}$, the net complex power from constant power sources $\mathfrak{s}_{m,t}$ at bus $m \in \mathcal{N}^{\text{pv}}_+ \bigcup \mathcal{N}^{\text{pump}}_+ \bigcup \mathcal{N}^{\text{c}}_+ \subseteq \mathcal{N}_+$ at time t then becomes

$$\mathfrak{s}_{m,t} = s^{\text{pv}}_{m,t} - \hat{s}^{\text{pump}}_{m,ij,t} - s^c_{m,t} \tag{21}$$

where if a PV inverter, pump, or load is not present at bus m, the corresponding term is omitted from (21). The WDN and PDN are coupled by (21) with $\hat{s}^{\text{pump}}_{m,ij,t}$ as the *coupling variable*. Since $\hat{p}^{\text{pump}}_{m,ij,t}$ is linear according to (8), it follows that (21) is a linear equality constraint.

The objective pertaining to PDN at time t is denoted by $\hat{C}_t$ and different choices are considered in Section 4. The multi-period optimal water power flow problem is presented next.

Multi-Period Optimal Water Power Flow: Let $f_t = \{f_{ij,t}\}_{ij\in\mathcal{L}}$, $\hat{p}^{\text{pump}}_t = \{\hat{p}^{\text{pump}}_{ij,t}\}_{ij\in\mathcal{P}}$, $\hat{h}_t = \{\hat{h}_{ij,t}\}_{ij\in\mathcal{L}}$, $h_t = \{h_{j,t}\}_{j\in\mathcal{M}}$, $x_t = \{x_{ij,t}\}_{ij\in\mathcal{P}}$, $s^{\text{pv}}_t = \{s^{\text{pv}}_{m,t}\}_{m\in\mathcal{N}^{\text{pv}}_+}$, $\hat{s}^{\text{pump}}_t = \{\hat{s}^{\text{pump}}_{m,ij,t}\}_{m\in\mathcal{N}^{\text{pump}}_+}$, $I_t = \{I_{nm,t}\}_{nm\in\mathcal{E}}$, $S_t = \{S_{nm,t}\}_{nm\in\mathcal{E}}$, $V_t = \{v_{n,t}\}_{n\in\mathcal{N}_+}$. The multi-period optimal water power flow problem is formulated involving two groups of variables defined as follows: $w_t := \{f_t, \hat{p}^{\text{pump}}_t, \hat{h}_t, h_t, x_t\}$, $y_t := \{V_t, I_t, S_t, s^{\text{pv}}_t, \hat{s}^{\text{pump}}_t\}$. The OWPF problem (P3) can be stated as follows

$$\text{(P3)}\quad \min \quad \sum_{t=1}^{T}\left[\lambda^{\text{WDN}}_t \sum_{ij\in\mathcal{P}} \bar{r}^{\text{pump}}_{ij,t}\right] + \sum_{t=1}^{T}\left[\lambda^{\text{PDN}}_t \hat{C}_t\right] \tag{22a}$$

$$\text{over} \quad \{w_t\}_{t=1}^T, \{y_t\}_{t=1}^T,\ t \in \mathcal{T}$$

$$\text{subj. to} \quad \text{(1a), (1c), (1g), (1h), (2), (6), (8), (11)}$$

$$\text{(14), (19), (20), (21), (15),(16), (17), (18)} \tag{22b}$$

where λ^{PDN}_t is the PDN time-varying price for electricity. Notice that the continuous part of the OWPF problem (P3) is nonconvex due to (16). Dropping (16) renders the continuous part of the problem convex and the formulation is called C-OWPF. In Section 4, an exactness check is performed to verify that the results obtained from solving C-OWPF are close to satisfying the rank-1 condition.

The C-OWPF problem amounts to a mixed-integer semidefinite program (MISDP). Although the computational effort required to solve the convex optimal water flow problem (C-OWF) (P2) is significantly reduced due to the successive linearizations that capture the unknown water flow directions without the use of additional binary variables, solving the C-OWPF problem (P3) as MISDP in a reasonable time using off-the-shelf solvers such as YALMIPs' built-in branch-and-bound (BNB) is still challenging; see e.g., [12] for experience with a different MISDP. Additionally, solving centralized problem formulations that necessitate a single authority overseeing and controlling the entire multi-energy infrastructure, i.e., WDN and PDN, may overall not be tenable in terms of data sharing and privacy concerns. Thus, to protect the data privacy of each energy system and efficiently solve the C-OWPF problem, Benders decomposition is used. This is the theme of the following section.

3. Benders-based C-OWPF solver

This section develops a distributed solver for the C-OWPF problem using Benders decomposition following ([20], Ch. 3) and [21]. The C-OWPF problem is decomposed into a *master problem* and a *subproblem* and the two problems are solved sequentially. In the present setting, the Benders decomposition is designed such that the *master problem* is solved by the WDN operator, and the PDN operator solves the *subproblem*. By fixing the *coupling variable*, i.e., $\hat{p}^{\text{pump}}_t$ (implicitly $\hat{s}^{\text{pump}}_t$) in the *subproblem*, the WDN and PDN operators solve smaller optimization problems in terms of the variables associated with their respective network and control devices. These optimization problems amount to a BFM-SDP OPF for the PDN *subproblem*, and a MILP C-OWF for the WDN operator *master problem*, thereby avoiding the aforementioned complexity in solving the MISDP C-OWPF. The formulations of Benders *master problem* and *subproblem* are presented next.

Subproblem: The *master problem* is time-coupled, where the coupling across time periods appears only due to tank dynamics (1c). Decomposing the C-OWPF problem into *master problem* and *subproblem* alleviates the time coupling in the *subproblem*. This feature is a consequence of the fact that no time coupling constraints pertain to the PDN. Therefore, the *subproblem* is formulated as (23) and is solved in parallel for each time period $t \in \mathcal{T}$. All variables in the *subproblem* pertain to Benders iteration ζ:

$$\text{(P4)}\quad \min \quad \text{U}^\zeta_t = \lambda^{\text{PDN}}_t \hat{C}^\zeta_t \tag{23a}$$

$$\text{over} \quad y^{\text{SP}}_t$$

$$\text{subj. to} \quad \text{(11), (14), (19), (20), (21), (15),(16), (17), (18)} \tag{23b}$$

$$\hat{p}^{\text{pump},\zeta}_t = \hat{p}^{\text{pump,fixed}}_t : \varrho^{\text{pump},\zeta}_t,\ t \in \mathcal{T} \tag{23c}$$

The optimization variables pertaining to each *subproblem* are collected in the vector y^{SP}_t defined as

$$y^{\text{SP}}_t := \{V^\zeta_t, I^\zeta_t, S^\zeta_t, s^{\text{pv},\zeta}_t, \hat{s}^{\text{pump},\zeta}_t, \varrho^{\text{pump},\zeta}_t\}$$

Constraint (23c) fixes variables $\hat{p}_t^{\text{pump}}$ to a fixed value $\hat{p}_t^{\text{pump,fixed}}$ obtained from the solution of the *master problem*. Denote $\hat{p}_t^{\text{pump,fixed}} = \{\hat{p}_{ij,t}^{\text{pump,fixed}}\}_{ij\in\mathcal{P}}$. The dual variables $\varrho_t^{\text{pump},\zeta}$ associated with (23c) provide sensitivities to be used in building Benders cuts for the *master problem*. Also note that $\varrho_t^{\text{pump},\zeta} = \{\varrho_{ij,t}^{\text{pump},\zeta}\}_{ij\in\mathcal{P}}$.

It is worth noting that the *subproblem* amounts to a BFM-SDP OPF with an additional linear constraint (23c) and is an SDP that can be efficiently solved using off-the-shelf solvers such as SeDuMi or Mosek.

The optimal objective value of the *subproblem* is calculated as follows in (24) to be used later in (25) and *master problem* (26).

$$\mathrm{U}^{\zeta} = \sum_{t\in\mathcal{T}} \mathrm{U}_t^{\zeta} \tag{24}$$

Note that *subproblem* is a restricted version of the original MISDP C-OWPF problem. Therefore, the upper bound for the optimal value of the objective function of the original MISDP C-OWPF problem at iteration ζ is given below:

$$\mathrm{U}_{\text{up}}^{\zeta} = \mathrm{U}^{\zeta} + \sum_{t=1}^{T}\left[\lambda_t^{\text{WDN}} \sum_{ij\in\mathcal{P}} \tilde{I}_{ij,t}^{\text{pump},\zeta}\right] \tag{25}$$

Master Problem: The *master problem* is formulated next, where all variables refer to Benders iteration ζ:

$$\text{(P5)} \quad \min \quad \mathrm{U}_{\text{lb}}^{\zeta} = \sum_{t=1}^{T}\left[\lambda_t^{\text{WDN}} \sum_{ij\in\mathcal{P}} \tilde{I}_{ij,t}^{\text{pump}(\zeta)}\right] + \theta^{\zeta} \tag{26a}$$

$$\text{over} \quad \{w_t^{\text{MP}}\}_{t=1}^{T}$$

$$\text{subj. to} \quad \text{(1a), (1c), (1g), (1h), (2), (6), (8)} \tag{26b}$$

$$\theta^{\zeta} \geq \theta^{\text{lb}} \tag{26c}$$

$$\mathrm{U}^{\tilde{\zeta}} + \sum_{ij,t} \varrho_{ij,t}^{\text{pump},\tilde{\zeta}}\left(\hat{p}_{ij,t}^{\text{pump},\zeta} - \hat{p}_{ij,t}^{\text{pump},\tilde{\zeta}}\right) \leq \theta^{\zeta}$$

$$\tilde{\zeta} = 1, \ldots, \zeta - 1 \tag{26d}$$

The optimization variables pertaining to the *master problem* are collected in the following optimization vector:

$$w_t^{\text{MP}} := \{f_t^{\zeta}, \hat{p}_t^{\text{pump},\zeta}, \hat{h}_t^{\zeta}, h_t^{\zeta}, x_t^{\zeta}, \theta^{\zeta}\} \tag{27}$$

Constraint (26d) includes Benders cuts previously generated in all previous Benders iterations through $\zeta - 1$. The Benders cuts are built using the primal variables $\hat{p}_{ij,t}^{\text{pump},\tilde{\zeta}}$ and dual variables $\varrho_{ij,t}^{\text{pump},\tilde{\zeta}}$ passed from the solution of the *subproblem* for $\tilde{\zeta} = 1, \ldots, \zeta - 1$. Constraint (26c) imposes a lower bound θ^{lb} on θ^{ζ}, which represents the objective value of the subproblem, and can be determined from physical or economical considerations [20]. Constraint (26c) is necessary to avoid unboundedness of the *master problem* when $\zeta = 1$. *Master problem* (P5) is a MILP that can be efficiently solved using off-the-shelf solvers such as Gurobi.

The *master problem* is a relaxed version of the original MISDP C-OWPF. Therefore, the objective function value $\mathrm{U}_{\text{lb}}^{\zeta}$ of the *master problem* is a lower bound for the optimal objective function value of the MISDP C-OWPF. Upon solving the *master problem*, the values of the coupling variables are updated. Specifically, the resulting optimal solution $\hat{p}_t^{\text{pump},\zeta}$ is passed on to the *subproblem* as $\hat{p}_t^{\text{pump,fixed}}$.

It is worth emphasizing that for each Benders iteration ζ, a sequence of problems (P5) is actually solved to update the parameters $\kappa_{ij,t}$, $\tau_{ij,t}$, $\psi_{ij,t}$, $\alpha_{ij,t}$, and $\beta_{ij,t}$ necessary to successively approximate the nonlinear pipe and pump head loss, as described in Section 2.

Note that it is possible for the *subproblem* to be infeasible for a given value of the coupling variable passed on from the *master problem*. In such cases, the literature suggests formulating an *always-feasible subproblem* without using additional Benders feasibility cuts in the *master problem* [20,21]. In the present work, the *subproblem* is feasible for the case studies under consideration.

Benders-based C-OWPF Solver: The detailed implementation is summarized in Algorithm 1. The PDN and WDN operators initially acquire the topology and operational constraints of their respective networks. The WDN operator solves a sequence of instances of the *master problem* (P5) in Step 4 through 12 and passes the resulting $\{\hat{p}_t^{\text{pump}}\}_{t=1}^{T}$ to the PDN operator during the first Benders iteration. Following that, the PDN operator solves the *subproblem* pertaining to each time t, i.e., Steps 14 and 15, obtains the sensitivities associated with the fixing constraint (23c), and communicates $\{\varrho_t^{\text{pump},\zeta}\}_{t=1}^{T}$ to the WDN operator in Step 17. As the iterations continue, the two operators exchange information about the shared variables to reach a consensus on the amount of power consumed by the pumps, and the algorithm terminates in Step 20. It is worth noting that as the number of Benders iterations (ζ) increases, the optimal value of θ^{ζ} converges to (24), i.e., U^{ζ}.

Algorithm 1: Benders-based C-OWPF Algorithm

Input : PDN operator acquires PDN topology and WDN operator acquires WDN topology along with their respective operational constraints

Output: $\{w_t^{\text{MP}}, y_t^{\text{SP}}\}_{t=1}^{T}$

1 Initialize $\zeta = 0$, small tolerance (tol = 0.0001) to control convergence, maxIter to 100, $\theta^{\text{lb}} = 0$, and $\mathrm{U}_{\text{up}}^{0} = \infty$, $\mathrm{U}_{\text{lb}}^{0} = -\infty$, set $\zeta = 1$;

2 Initialize variables in (27) and place them in $\langle\{w_t^{\text{MP}}\}_{t=1}^{T}\rangle_{\text{save}}$;

3 **while** $|\mathrm{U}_{\text{up}}^{\zeta} - \mathrm{U}_{\text{lb}}^{\zeta}| \geq$ tol *OR* $\zeta \leq$ maxIter **do**

4 Initialize successive iteration counter $\omega = 1$ and $\Delta = \infty$ **while** $\Delta \geq$ successive tolerance = 0.5 **do**

5 Update parameters of (6a), (6b), (8) using $\langle\{w_t^{\text{MP}}\}_{t=1}^{T}\rangle_{\text{save}}$;

6 WDN operator solves MILP *master problem* (P5);

7 Set $\langle\{w_t^{\text{MP}}\}_{t=1}^{T}\rangle_{\omega}$ as the solution of (P5);

8 Calculate $\Delta := \text{norm}[\langle\{w_t^{\text{MP}}\}_{t=1}^{T}\rangle_{\omega} - \langle\{w_t^{\text{MP}}\}_{t=1}^{T}\rangle_{\text{save}}]$;

9 Update $\langle\{w_t^{\text{MP}}\}_{t=1}^{T}\rangle_{\text{save}} = \langle\{w_t^{\text{MP}}\}_{t=1}^{T}\rangle_{\omega}$, and $\omega \leftarrow \omega + 1$

10 **end**

11 Set $\{w_t^{\text{MP},\zeta}\}_{t=1}^{T} = \langle\{w_t^{\text{MP}}\}_{t=1}^{T}\rangle_{\text{save}}$;

12 Communicate $\{\hat{p}_t^{\text{pump,fixed}}\}_{t=1}^{T}$ to PDN operator

13 **for** $t = 1 : \mathrm{T}$ **do**

14 PDN operator solves the *subproblem* (P4) as SDP and computes $\varrho_t^{\text{pump},\zeta}$;

15 Set $y_t^{\text{SP},\zeta}$ as the solution of (P4)

16 **end**

17 Communicate $\{\varrho_t^{\text{pump},\zeta}\}_{t=1}^{T}$ to WDN operator;

18 Calculate $\mathrm{U}_{\text{up}}^{\zeta}$ and $\mathrm{U}_{\text{lb}}^{\zeta}$ and set $\zeta \leftarrow \zeta + 1$

19 **end**

20 The PDN operator issues setpoints to PV inverters, and the WDN operator issues scheduling decisions to pumps.

Remark 1. *Computational complexity of iterative master problem.* The water flows in pipes generally change direction during the scheduling horizon. To deal with this issue, the literature either assumes prior knowledge of the flow directions [4,6], or a binary variable is introduced per pipe to encode the unknown direction [5]. In contrast, the proposed formulation in *master problem* that relies on the successive linearizations in [2,13] can capture the unknown flow directions *without the need for additional binary variables*. As an example, for scheduling a network with $|\mathcal{P}|$ pumps and $|\mathcal{W}|$ pipes over $|\mathcal{T}|$ time periods, the work in [5] entails $|\mathcal{T}||\Theta|(|\mathcal{P}| + |\mathcal{W}|)$ binary variables, where $|\Theta|$ denotes the number of segments used to linearize the pump and pipe curves. In contrast, our proposed formulation in the *master problem* requires only $|\mathcal{T}||\mathcal{P}|$ binary variables. Considering that the number of pipes in typical WDNs is significantly larger than the number of pumps, the computational savings are noteworthy.

4. Numerical tests

This section evaluates the efficacy of Benders-based C-OWPF in terms of joint objective improvements over a decoupled design and a centralized C-OPWF solver in two test cases, namely, the IEEE 4-bus

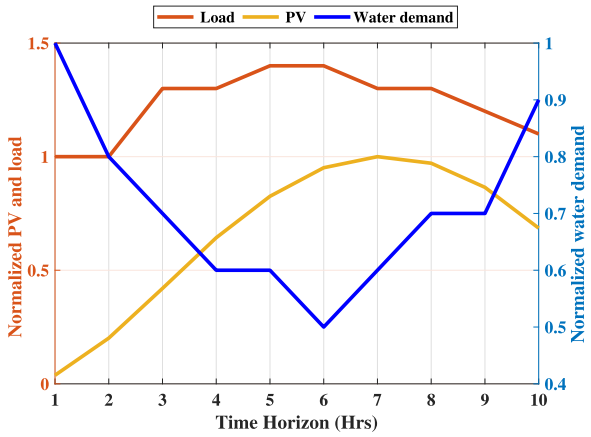

Fig. 2. Network-wide normalized PV, load, and water demand profiles for Test Case A.

PDN coupled with a 3-node WDN (Test Case A) and the IEEE 123-bus PDN coupled with the 36-node WDN (Test Case B). In particular, Test Case A compares the performance of Benders-based C-OWPF with the decoupled design that utilizes the conventional rule-based control for WDNs implemented in EPANET [15]; resultant pump schedules are then passed to solve the SDP-based OPF problem. Test Case B features a comparison of Benders-based C-OWPF with the centralized C-OWPF solver. The *master problem* in Benders-based C-OWPF is solved using Gurobi and the *subproblem* is solved using Mosek with CVX. The centralized C-OWPF problem is solved using Gurobi in YALMIP.

All simulations are run on a 2.30-GHz, intel core i7 computer with 192 GB of RAM. The head unit is feet [ft]; and the flow unit is gallons per minute [GPM]. The slack bus voltage is fixed to $v^{\text{nom}} = \{1, 1\angle -120°, 1\angle 120°\}$ per unit [pu]. The pump motor operates with PF = 0.9. The pipe lengths, diameters, node elevations, tank diameter, and junction base demands are obtained from [13,15] for the 3-node and 36-node WDN, respectively. The 36-node WDN in EPANET corresponds to Net 2 network, which corresponds to a small region of the Cherry Hill/Brushy Plains WDN.

Test Case A: IEEE 4-bus PDN coupled with 3-node WDN

The modified IEEE 4-bus PDN [9] and modified 3-node WDN [13] are depicted in Fig. 1. The system is operated over a time horizon of $T = 10$ h, beginning at 6 am with δ as one hour. For the PDN, V_{base} is 12.47 kV line-to-line and S_{base} is 6 MVA. The bounds on pump flows are selected as $[f_{\min}, f_{\max}] = [0, 20\,000]$ GPM. The tank minimum height, maximum height, and initial level are respectively set to $h_{\min} = 900$ ft, $h_{\max} = 950$ ft, and $h_0 = 905$ ft. Furthermore, we consider an FSP with parameters $h_0 = 533.4$ ft, $\sigma = 1.334 \times 10^{-6}$, and $\nu = 2$ computed from EPANET [15]. Similarly, the line, transformer parameters, and nominal loads of the modified 4-bus PDN are obtained from [9], wherein one PV inverter is located at bus number 3. Using the default parameters on NRELs' PVWatts [22] with ZIP code 78249 for San Antonio, Texas, USA, the ac power production of a PV system with 1600 kW size is obtained for July 23, 2021, from 6 am–4 pm. Furthermore, we assume $\mathbf{s}^{\text{pv}}_{\max}$ to be 125% of $\mathbf{p}^{\text{pv}}_{\max}$. The bounds on the squared magnitude voltage (18) are respectively set to $(0.95)^2$ and $(1.05)^2$ (p.u.)^2. The nominal load at bus number 4 in PDN is further divided into 40% for baseload and 60% for pumping load, respectively. Fig. 2 depicts the network-wide load, PV, and water demand profiles for the case study. The values of λ^{WDN}_t and λ^{PDN}_t are chosen to be 1. In this test case, the active power losses across the lines of the PDN are minimized, that is, the objective function for the PDN is $\hat{C}_t = \hat{C}^{\text{loss}}_t$ where $\hat{C}^{\text{loss}}_t = \sum_{(n,m)\in\mathcal{E}} \text{Tr}(\text{Re}(Z_{nm} I_{nm,t}))$ [12].

The decoupled design in this test case consists of two stages and is similar to that discussed in [2]. For easier reference, we refer to the decoupled problem, as Scenario I; and the Benders-based C-OWPF is referred to as Scenario II.

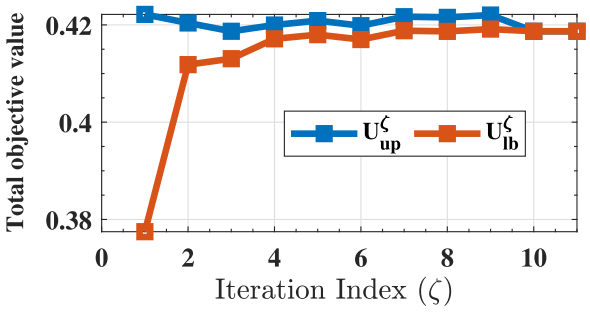

Fig. 3. Convergence of Benders-based C-OWPF problem in Test Case A.

Table 1
Comparison of objective function values (in p.u.) for Scenario I and Scenario II in Test Case A.

Objective function	Scenario I	Scenario II	% Reduction
$\sum_t \sum_{ij\in\mathcal{P}} \Gamma^{\text{pump}}_{ij,t}$	0.5080	0.3750	26.18
$\sum_t \hat{C}^{\text{loss}}_t$	0.050	0.0437	12.6
Total objective	0.5580	0.4180	25.09

Table 1 summarizes the achieved cost in the two scenarios. It is worth noting that EPANET (Scenario I) calculates the nonlinear pump power as specified in (4). On the other hand, Scenario II computes an approximate value for the pump power. To ensure a fair comparison, the optimal pump schedules computed by Scenario II are entered into EPANET to determine the actual nonlinear pump power. From Table 1, it is evident that Scenario II enhances the flexibility, which reduces the total objective value compared with Scenario I. For example, the *total objective* value is respectively reduced by 25.09%. The % reductions in operational costs are primarily achieved due to operating FSPs during times of low water and power demand. Notably, in Scenario I, which is agnostic to the PDN load and PV production, requires the pump to run for hours 1 through 4 in order to comply with the rules. On the other hand, in Scenario II, the pump is turned on only at hours 2, 7, and 9, when PV generation in the PDN is high and water demand in the WDN is low.

The convergence of the Benders-based C-OWPF solver (Scenario II) is depicted in Fig. 3. The algorithm converges in Benders iteration 10, where the difference between $\text{U}^{\zeta}_{\text{up}}$ (upper curve) and $\text{U}^{\zeta}_{\text{lb}}$ (lower curve) is smaller than the allowed tolerance 0.0001. It is worth noting that theoretically, the lower bound should be monotonically increasing. Nevertheless, a small oscillation is observed in the lower curve of Fig. 3. Such small numerical issues are possible and have been reported in the literature before, see e.g., ([21], Fig. 5). The computational time required to solve the Benders-based C-OWPF Problem (Scenario II) is less than 15 min for the Test Case A. We also attempted to solve the MISDP-based C-OWPF problem (P3) using YALMIPs' built-in BNB solver in conjunction with MOSEK. The YALMIP-BNB solver did not converge convergence even when the number of BNB iterations was increased to 50 000. This finding corroborates the strength of the Benders-based C-OWPF capability to solve the multi-period MISDP.

Test Case B: IEEE 123-bus PDN coupled with 36-node WDN

The objective of this Test Case is two-fold: (1) to examine the impact of using a linearized approximate versus the relaxed power flow model on solving the optimal water power flow problem; and (2) to assess the scalability of the Benders-based C-OWPF method. Specifically, this test case compares the Benders-based C-OWPF developed in Section 3 which utilizes SDP-based relaxation for power flow equations with a C-OWPF solver which uses the $LinDist3Flow$ approximation for the power flow equations. The $LinDist3Flow$ has been used in [23] and other pertinent references to solve OPF problems for PV reactive power control. The $LinDist3Flow$ is also used in the context of optimal water power flow in multi-phase PDNs [3], albeit, the on/off

Table 2
WDN price ($\frac{\$}{\text{kWh}}$) in Test Case B.

Time (h)	1	2	3	4	5	6	7	8	9	10	11	12
λ_t^{WDN}	0.12	0.11	0.12	0.10	0.11	0.12	0.13	0.14	0.15	0.16	0.18	0.19
Time (h)	13	14	15	16	17	18	19	20	21	22	23	24
λ_t^{WDN}	0.19	0.2	0.21	0.22	0.23	0.23	0.2	0.18	0.2	0.17	0.13	0.12

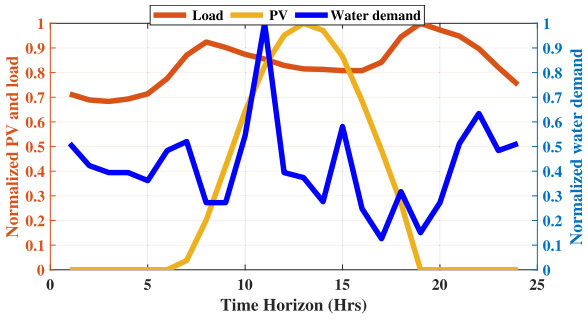

Fig. 4. Network-wide normalized PV, load, and water demand profiles for Test Case B.

schedules and water directions are assumed to be known. Therefore, the *LinDist3Flow* appears to be a promising model for power flow approximation.

To this end, the nonconvex power flow equations are replaced by their linear counterparts using the *LinDist3Flow* approximation upon ignoring losses and other high-order terms and assuming voltages are approximately balanced [23]. Then, using monomial approximations as described in Section 2 for the nonlinear hydraulics in WDNs, a convex optimal water power flow problem C-OWPF is formulated. Specifically, the *LinDist3Flow*-based C-OWPF is convex in the continuous variables, includes 0/1 pump scheduling decisions, and is solved iteratively due to the monomial approximations of the WDN hydraulics. The exact formulation is omitted due to space limitation.

The previously mentioned C-OWPF adopting the *LinDist3Flow* approximation is solved in a centralized fashion and is therefore referred to as centralized C-OWPF in this section. The centralized C-OWPF amounts to a large-scale mixed integer linear or quadratic programming problem, depending on the choice of objective function for the PDN. It is worth noting that the Benders-based C-OWPF solver is decentralized and thus ensures privacy of the respective WDN and PDN operators.

The modified IEEE 123-bus PDN [9] and modified 36-node WDN [13] are considered. The system is operated over a time horizon of $T = 24$ h, and δ is one hour. For the IEEE 123-bus PDN, transformers are modeled as wye-g–wye-g connections. Switches are replaced by short lines. Line shunt admittances and voltage regulators are ignored, however, capacitor banks are accounted for. The bounds on the squared magnitude voltage (18) are respectively set to $(0.95)^2$ and $(1.05)^2$ (p.u.)^2 in Benders-based C-OWPF. They are set to $(0.97)^2$ and $(1.05)^2$ (p.u.)^2 for the *LinDist3Flow*-based formulation of centralized C-OWPF to overcome the inaccuracy of the linear approximation. Furthermore, six PV inverters with a size of 1000 kW each are located at buses $\{13, 21, 25, 78, 86, 87\}$ with $s_{\text{max}}^{\text{pv}}$ set to 125% of $p_{\text{max}}^{\text{pv}}$. The PDN objective minimizes the real power import from the substation, that is, the objective function for the PDN is $\hat{C}_t = \hat{C}_t^{\text{import}}$ and $\hat{C}_t^{\text{import}} = \text{Re}(\mathbf{1}_3^{\top} s_{0,t})$, where $s_{0,t}$ represents the power flows leaving the substation at time t.

The 36-node WDN includes a reservoir with a fixed head of 100 ft and an FSP with parameters $h_0 = 400$ ft, $\sigma = 2.5 \times 10^{-5}$, and $\nu = 2$ computed from EPANET. Moreover, the pump is connected to bus 93 of the PDN. Fig. 4 depicts the network-wide water demand, real power load, and PV profiles considered in Test Case B, where the water demand profile is taken from EPANETs' 36-node WDN data; the load profile of PDN is adopted from [5]; and the PV profile is obtained from NRELs' PVWatts calculator for July 23, 2021. The WDN price, λ_t^{WDN}, is shown in Table 2 [14]. The PDN price λ_t^{PDN} is set to 1 for all t. The case of $\lambda_t^{\text{WDN}} = 1$ for all t is considered as well.

The objective values listed in Table 3 are calculated using the respective nonlinear solvers, namely, Z-Bus method for PDN [18] and EPANET for WDN. Specifically, $\sum_t \sum_{ij \in \mathcal{P}} I_t^{\text{pump}}$ in Table 3 corresponds to the actual pump power determined by EPANET upon fixing the pump schedules achieved by each solver for each price scenario. The actual power import objective $\sum_t C_t^{\text{import}}$ is calculated by passing the optimal reactive power setpoints of PV inverters and the actual pump powers computed by the respective methods. Table 4 lists the pump on/off statuses with time-varying (top rows) and constant WDN price (bottom rows).

The following key observations for Test Case B are highlighted.

- The on/off schedules reported in Table 4 for Benders-based C-OWPF and centralized C-OWPF are different.
- Under time-varying WDN price, the Benders-based C-OWPF turns on the pump during low load and high PV generation, i.e., hours 10—12, despite the high WDN price and water demand at hours 10 and 11. Compared to the centralized C-OWPF, this leads to a slight increase of about 0.36% in pump power consumption and a 2.9% drop in power import objective. The overall percent reduction is 2.83%, the majority of which is attributed to decrease in the power import objective. Interestingly, the pump is turned on during hour 11 by the Benders-based C-OWPF and centralized C-OWPF. The centralized C-OWPF turns on the pump during low water demand, i.e., hours 1, 5, and 6, but not during high PV generation, such as hour 12. This behavior can possibly be attributed to the fact that the centralized C-OWPF uses the *LinDist3Flow*, which ignores line losses and other higher-order terms and may therefore render the voltage constraints inactive. However, higher-order terms can be included to improve the optimality of *LinDist3Flow* at the expense of solving the *LinDist3Flow* OPF iteratively [23]—which is not presently carried out in the centralized C-OWPF solver. This highlights the benefits of the SDP-based relaxations for solving large-scale OWPF problems in multi-phase PDNs using Benders' decomposition.
- Under constant WDN price, a similar pattern is observed as mentioned previously. Overall, the Benders-based C-OWPF achieves a 3.13% reduction in the total objective value when compared to the centralized C-OWPF.
- Table 5 reports the computational time required to solve the Benders-based C-OWPF and centralized C-OWPF under time-varying WDN price as 17 min and 35 min respectively. The Benders-based C-OWPF converges in three iterations as depicted in Fig. 5. For each Benders' iteration, the *masterproblem* is solved in less than 5 min, and the set of time-decoupled *subproblems* is solved in less than 40 s. The SDP implementation of the *subproblem* is based on Github codes available at the link in [11]. The *parallelcomputingtoolbox* of MATLAB is used to reduce the *subproblem* computational time. Furthermore, because the centralized C-OWPF amounts to solving a sequence of large-scale MILPs, the *optimizer* block of YALMIP is used to speed up the centralized C-OWPF, which prevents the same optimization problem from being built multiple times. With constant WDN price, the computational time reported by the Benders-based C-OWPF is 30 min. In

Table 3
Objective function values (in p.u.) for Benders-based C-OWPF and the centralized C-OWPF in Test Case B. The % reduction is with respect to the centralized C-OWPF.

WDN price	Method	$\sum_t \sum_{ij\in\mathcal{P}} \Gamma_{ij,t}^{\text{pump}}$	$\sum_t C_t^{\text{import}}$	Total
Time varying λ_t^{WDN}	Benders-C-OWPF	0.1365	6.1448	6.2813
	Centralized C-OWPF	0.1360	6.3283	6.4643
	% reduction	−0.36	2.9	2.83
$\lambda_t^{\text{WDN}} = 1$	Benders-C-OWPF	0.1367	6.1440	6.2807
	Centralized C-OWPF	0.1362	6.3522	6.4844
	% reduction	−0.36	3.2	3.13

Table 4
Pump *on/off* decisions in Test Case B under time-varying (top rows) and constant (bottom rows) WDN price.

Time (h)	1	2	3	4	5	6	7	8	9	10	11	12	13	14	15	16	17	18	19	20	21	22	23	24
Benders C-OWPF	0	1	0	1	0	0	0	0	0	1	1	1	0	0	0	0	0	0	0	0	0	0	0	0
Centralized C-OWPF	1	0	0	1	1	1	0	0	0	0	1	0	0	0	0	0	0	0	0	0	0	0	0	0
Benders C-OWPF	1	0	0	0	0	1	0	0	0	0	1	1	1	0	0	0	0	0	0	0	0	0	0	0
Centralized C-OWPF	1	1	0	0	0	0	0	1	0	1	1	0	0	0	0	0	0	0	0	0	0	0	0	0

this case, the Benders-based C-OWPF converges in six iterations. The computational time reported by the centralized C-OWPF is 38 min, which is slightly higher than the corresponding time of the Benders-based C-OWPF.

- The minimum and maximum magnitudes across all time periods and buses of the voltage profile $\check{v}$ corresponding to actual power flows computed by the Z-Bus method are reported in Columns 3 and 4 of Table 5. Both Benders-based and the centralized C-OWPF methods report feasible voltages.
- Since Benders-based C-OWPF employs SDP relaxation of the power flow equations, the optimality gap is assessed in Table 6. The % Gap in last row of Table 6 is defined as Gap $= \frac{\sum_t C_t^\zeta - \sum_t \hat{C}_t^\zeta}{\sum_t \hat{C}_t^\zeta} \times 100\%$ (assuming $\lambda_t^{\text{PDN}} = 1$), where the objective lower bound $\sum_t \hat{C}_t^\zeta$ is computed by the *subproblem* for each Benders' iteration ζ. A feasible objective value $\sum_t C_t^\zeta$ is obtained from actual power flows computed with the Z-Bus method using the PV setpoints and pump powers of the *subproblem* at iteration ζ. It is worth noting that the Benders-based C-OWPF exhibits *practically zero optimality gap* at every iteration. For completeness, the optimality gap pertaining to the $LinDist3Flow$ approximation of the centralized C-OWPF is evaluated against the SDP relaxation of Benders-based C-OWPF in the last column of Table 5. The feasible objective value from $Lindist3Flow$ $\sum_t C_t$ is computed based on the actual power flows, using the setpoints produced by the centralized C-OWPF. The lower bound is provided by the SDP relaxation $\sum_t \hat{C}_t$. The $LinDist3Flow$ yields an optimality gap of 2.9% and 3.42% under time-varying and constant WDN prices, respectively.
- Another approach to assess the quality of the SDP relaxation in the *subproblem* is to check the ratio of the second largest to the largest eigenvalue for each PSD matrix [10]. For all PSD matrices in Test Cases A and B, the eigenvalue ratio over the scheduling horizon is very small; for instance, it is less than 0.81×10^{-09} at the final Benders' iteration. The small ratio confirms that the relaxation is tight.
- Due to the fact that the WDN hydraulics are approximated using successive linearizations, the modeling accuracy is assessed by comparing the resulting flows, heads, and pump power consumptions to the nonlinear hydraulics produced by EPANET. For the Test Cases A and B, the two models, i.e., the monomial approximations and the EPANET agree on nodal heads and flows to within 0.001 ft and 0.02 GPM, respectively. The approximated pump powers differ from the ones of EPANET by no more than 0.05 kW.

Table 5
Minimum and maximum voltage magnitudes (p.u.), computational time (min), and optimality gap (%) for Benders-based C-OWPF and the centralized C-OWPF in Test Case B.

WDN price	Method	min ($\check{v}$)	max ($\check{v}$)	Time	% Gap
Time varying λ_t^{WDN}	Benders-C-OWPF	0.95	1.05	17	0
	centralized C-OWPF	0.952	1.04	35	2.9
$\lambda_t^{\text{WDN}} = 1$	Benders-C-OWPF	0.95	1.04	30	0
	centralized C-OWPF	0.953	1.043	38	3.42

Table 6
Optimality gap for SDP *subproblem* in Benders-based C-OWPF in Test Case B under time-varying WDN price.

Benders' iteration ζ	1	2	3
$(\sum_t \hat{C}_t)^\zeta$	6.1496	6.1446	6.1448
$(\sum_t C_t)^\zeta$	6.1496	6.1446	6.1448
% Gap	0	0	0

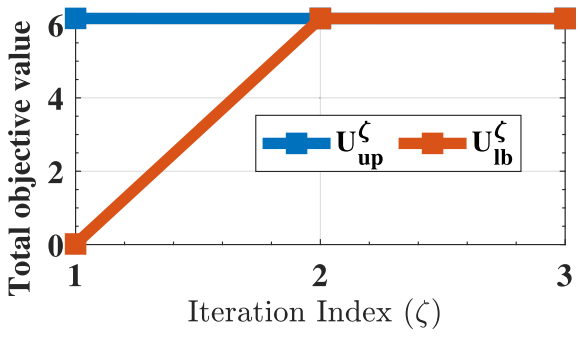

Fig. 5. Benders-based C-OWPF convergence for Test Case B with time-varying WDN price.

5. Conclusions and future directions

This paper proposes a convex multi-period scheduling framework called C-OWPF to optimally operate pumps in WDNs and PV inverters in multi-phase distribution networks accounting for the coupling between two infrastructures. The C-OWPF problem can be solved as a MISDP. The capability of modern MISDP solvers in obtaining tractable solutions is still limited. To this end, this paper leverages Benders decomposition to circumvent the tractability issues inherent in the MISDP-based C-OWPF while allowing the WDN and PDN operators to pursue individual objectives respecting the coupling between the two networks. The numerical results evince the effectiveness of the

proposed Benders-based C-OWPF solver compared to a traditional rule-based decoupled approach and a centralized C-OWPF solver adopting the *LinDist3Flow* approximation for the power flow equations. Computation time reductions with implementation of the Benders-based C-OWPF solver in the open-source programming language Julia will be explored in the future. Future work will also incorporate variable-speed pumps and pressure-reducing valves in WDNs as well as step-voltage regulators and energy storage in multi-phase PDNs. Stochastic frameworks to account for the uncertainties of power consumption, water demands, and PV renewable power are worth exploring as well.

CRediT authorship contribution statement

Krishna Sandeep Ayyagari: Conceptualization, Methodology, Software, Writing – original draft. **Nikolaos Gatsis:** Conceptualization, Writing – review & editing, Supervision.

Declaration of competing interest

The authors declare that they have no known competing financial interests or personal relationships that could have appeared to influence the work reported in this paper.

References

[1] E. Dall'Anese, P. Mancarella, A. Monti, Unlocking flexibility: Integrated optimization and control of multienergy systems, IEEE Power Energy Mag. 15 (1) (2017) 43–52.

[2] K.S. Ayyagari, S. Wang, N. Gatsis, A.F. Taha, M. Giacomoni, Co-optimization of interdependent water and power distribution networks, in: Proc. IEEE Power Energy Society Innovative Smart Grid Technologies Conference (ISGT), Washington, DC, USA, 2021, pp. 1–5.

[3] A. Stuhlmacher, J.L. Mathieu, Water distribution networks as flexible loads: A chance-constrained programming approach, Electr. Power Syst. Res. 188 (2020) 106570.

[4] A. Stuhlmacher, J.L. Mathieu, Chance-constrained water pumping to manage water and power demand uncertainty in distribution networks, Proc. IEEE 108 (9) (2020) 1640–1655.

[5] K. Oikonomou, M. Parvania, Optimal coordinated operation of interdependent power and water distribution systems, IEEE Trans. Smart Grid 11 (6) (2020) 4784–4794.

[6] A.S. Zamzam, E. Dall'Anese, C. Zhao, J.A. Taylor, N.D. Sidiropoulos, Optimal water–power flow-problem: Formulation and distributed optimal solution, IEEE Trans. Control Netw. Syst. 6 (1) (2019) 37–47.

[7] Y. Yao, C. Li, K. Xie, H.-M. Tai, B. Hu, T. Niu, Optimal design of water tank size for power system flexibility and water quality, IEEE Trans. Power Syst. 36 (6) (2021) 5874–5888.

[8] T.M. Walski, D.V. Chase, D.A. Savic, W. Grayman, S. Beckwith, E. Koelle, Advanced Water Distribution Modeling and Management, Civil and Environmental Eng. and Eng. Mechanics Faculty Pub., 2013.

[9] W.H. Kersting, Radial distribution test feeders, in: Proc. IEEE Power Eng. Soc. Winter Meet., Columbus, OH, 2001, pp. 908–912.

[10] L. Gan, S.H. Low, Convex relaxations and linear approximation for optimal power flow in multiphase radial networks, in: Proc. Power Systems Computation Conference, Wroclaw, Poland, 2014, pp. 1–9.

[11] M. Bazrafshan, N. Gatsis, H. Zhu, Optimal power flow with step-voltage regulators in multi-phase distribution networks, IEEE Trans. Power Syst. 34 (6) (2019) 4228–4239.

[12] I. Alsaleh, L. Fan, Multi-time co-optimization of voltage regulators and photovoltaics in unbalanced distribution systems, IEEE Trans. Sustain. Energy 12 (1) (2021) 482–491.

[13] S. Wang, A.F. Taha, L. Sela, M.H. Giacomoni, N. Gatsis, A new derivative-free linear approximation for solving the network water flow problem with convergence guarantees, Water Resour. Res. 56 (2020) e2019WR025694.

[14] S. Wang, A. Taha, N. Gatsis, M. Giacomoni, Receding horizon control for drinking water networks: The case for geometric programming, IEEE Trans. Control Netw. Syst. 7 (3) (2020) 1151–1163.

[15] L.A. Rossman, EPANET 2 User's Manual, Tech. Rep., Environmental Protection Agency, Washington, DC, USA, 2000.

[16] A.M. Gleixner, H. Held, W. Huang, S. Vigerske, Towards globally optimal operation of water supply networks, Numer. Algebra Control Optim. 2 (2012) 695–711.

[17] R. Menke, E. Abraham, P. Parpas, I. Stoianov, Exploring optimal pump scheduling in water distribution networks with branch and bound methods, Water Resour. Manag. 30 (14) (2016) 5333–5349.

[18] M. Bazrafshan, N. Gatsis, Comprehensive modeling of three-phase distribution systems via the bus admittance matrix, IEEE Trans. Power Syst. 33 (2) (2018) 2015–2029.

[19] W.H. Kersting, Distribution System Modeling and Analysis, fourth ed., CRC Press, Boca Raton, FL, USA, 2018.

[20] A. Conejo, E. Castillo, R. Mínguez, R. García, Decomposition Techniques in Mathematical Programming Engineering and Science Applications, Springer, Heidelberg, Germany, 2006.

[21] A. Nasri, S.J. Kazempour, A.J. Conejo, M. Ghandhari, Network-constrained AC unit commitment under uncertainty: A benders' decomposition approach, IEEE Trans. Power Syst. 31 (1) (2016) 412–422.

[22] National Renewable Energy Laboratory, PVWatts Documentation. [Online]. Available: https://pvwatts.nrel.gov/.

[23] B.A. Robbins, A.D. Domínguez-García, Optimal reactive power dispatch for voltage regulation in unbalanced distribution systems, IEEE Trans. Power Syst. 31 (4) (2016) 2903–2913.